INSTITUTE OF PHYSICS PUBLISHING and INTERNATIONAL ATOMIC ENERGY AGENCY NUCLEAR FUSION

Nucl. Fusion **45** (2005) 581–587 doi:10.1088/0029-5515/45/7/005

Modelling of ITER improved H-mode operation with the integrated core pedestal SOL model

G.W. Pacher[1], H.D. Pacher[2], G. Janeschitz[3], A.S. Kukushkin[4], A. Pankin[5], G. Pereverzev[6] and I. Voitsekhovitch[7]

[1] Hydro-Québec, 1804 mtee. L. Boulet, Varennes, Québec, J3X 1S1, Canada
[2] INRS-EMT, Varennes, Québec, Canada
[3] FZK-PL-Fusion, Karlsruhe, Germany
[4] ITER IT, Garching, Germany
[5] SAIC, San Diego, USA
[6] Max-Planck Institut für Plasmaphysik, Garching, Germany
[7] Euratom/UKAEA Fusion Association, Abingdon, UK

E-mail: pacher.guenther@ireq.ca

Received 8 December 2004, accepted for publication 10 May 2005
Published 23 Jun 2005
Online at stacks.iop.org/NF/45/581

Abstract
The hypothesis that improved H-modes result from reduction of transport where low-order rational surfaces are sparse is investigated with the integrated core pedestal SOL model. A function which expresses this sparseness is defined and a strength of reduction is determined which reproduces the improvement in confinement observed in Asdex-UG. The same dependence then agrees approximately with JET results. In application to ITER, the improved confinement gives improved fusion performance only if additional neoclassical impurity accumulation can be reduced or eliminated.

PACS numbers: 52.55Fa, 28.52Av

1. Introduction

The integrated core pedestal SOL (ICPS) model first introduced in [1] has been continuously modified and improved [2–4]. Anomalous core energy transport is now described with the multi-mode model [5], which includes transport contributions from ITG and TEM modes as well as from kinetic and resistive ballooning modes. In particular, we use the MMM95 module from [6]. Transport is assumed to be stabilized by a combination of $E \times B$ velocity shear and magnetic shear s as described in [4].

$$\chi = \frac{\chi_{\mathrm{MMM}}}{\{(1 + (\omega_{E\times B}/(G\gamma_0))^2) \cdot \max(1, (s-t)^2)\}},$$

where

$$\omega_{E\times B} = \frac{RB_\theta}{B}\frac{\partial}{\partial r}\left(\frac{E}{RB_\theta}\right) \qquad \text{and} \qquad E = \frac{\nabla p_i}{n_i e},$$

(where γ_0, the volume average of γ_{ITG} inside 0.9 of the minor radius, is an estimate of the growth rate in the absence of stabilization; $\omega_{E\times B}$ is the $E \times B$ shearing rate with R the major radius; and χ_{MMM} is the transport coefficient in the absence of stabilization). This stabilization leads to the formation of an edge pedestal. The stabilization parameters G and t are calibrated against experimental results of JET and Asdex-UG [4], for which a good fit is obtained with both parameters equal to 0.5. In the previous modelling [1–4], the anomalous particle transport was found to be well represented by $0.1(\chi_e + \chi_i)$. This expression is also used for the anomalous transport of impurity species. All transport coefficients are augmented by the neoclassical contributions. The effect of ELMs is represented in a time-averaged sense by limiting the pressure gradient to the ballooning limit [1]. The current density profile is determined using neoclassical resistivity (Hirshman formulation [7]), with increased resistivity inside the $q = 1$ surface to simulate the effect of sawteeth by flattening the profile. All results shown here are for fully relaxed current profiles, including non-inductive current drive as noted.

For ITER modelling, the boundary conditions (separatrix parameters) for the core model are self-consistently determined by scaling relationships, obtained from a database of B2-Eirene runs for the ITER SOL and divertor ([8, 9] and references therein). The model also includes neoclassical accumulation of the carbon intrinsic impurity [10], with a separatrix density determined from B2-Eirene modelling [9].

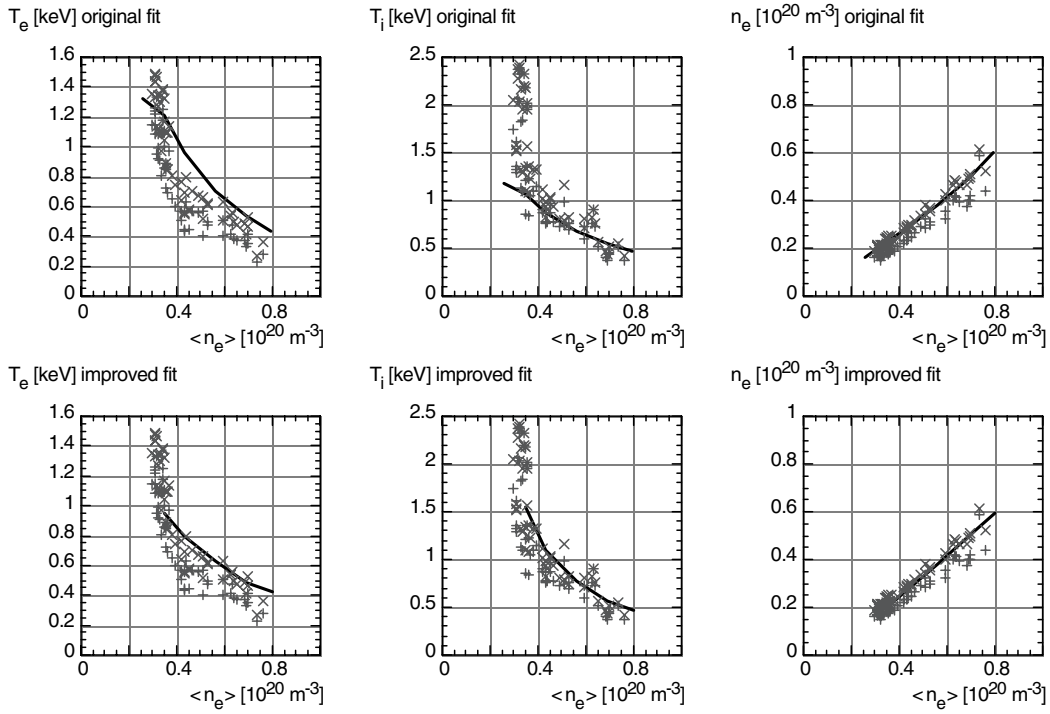

Figure 1. Comparison of simulations (black lines) with experimental database (grey symbols) for Asdex-UG for temperatures of electrons (left), ions (middle) and electron density (right). For the experiment, values at the outermost radius of the data (+) and at 95% of this radius (×) are shown. For the simulation, the values at the 95% flux surface are plotted. Top row shows the results without ETG and with the previously specified fuelling profile as in [4]. Bottom row shows the improved fit with ETG and with the corrected fuelling profile.

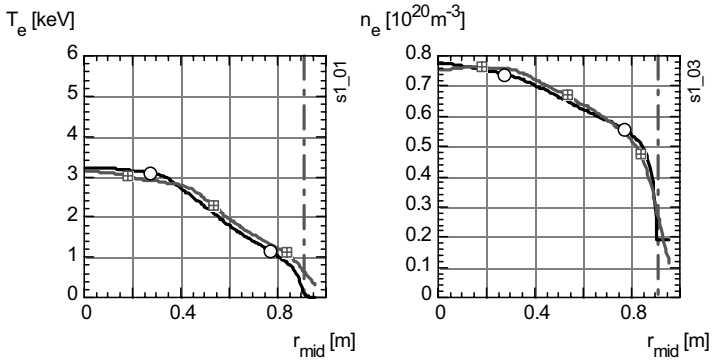

Figure 2. Comparison of simulations (black lines, circles) with experiment (grey lines, boxes) for JET.

2. Validation against Asdex-UG

In [4], it was noted that the pedestal electron temperatures predicted by the version of the model then used were systematically higher than the AUG experimental values, whereas the ion temperatures showed much better agreement. Following [11], an additional term corresponding to ETG transport was added to the electron heat transport coefficient. This term, which is not stabilized by flow shear, is calculated as in [11] from the Horton model [12] for short wavelength drift turbulence with electromagnetic effects.

Also, the beam particle source previously used was (erroneously) too small, by a factor of almost two, and this is now corrected. With these improvements, good agreement is now obtained for both electron and ion temperatures inside the pedestal in AUG. Figure 1 shows the comparison between the presently obtained edge parameters with those obtained in [4]. Note that, in [4], the edge parameters were plotted at a radius determined by a strong change in the slope of electron temperatures, whereas here, values at a fixed radius (95% flux surface) are plotted. The addition of ETG transport has no effect in the region limited by the ballooning limit. The 95% flux surface lies inside this region, so the addition of ETG transport increases the electron heat transport coefficient there. This method of plotting is more representative of the experimental data, which are clearly inside the pedestal region since the values at 100% and 95% of the radius (shown in figure 1) are almost the same. In JET, the corrected fuelling source results in a less flat density profile than obtained previously (figure 2). The agreement between model and experiment is seen to be improved significantly.

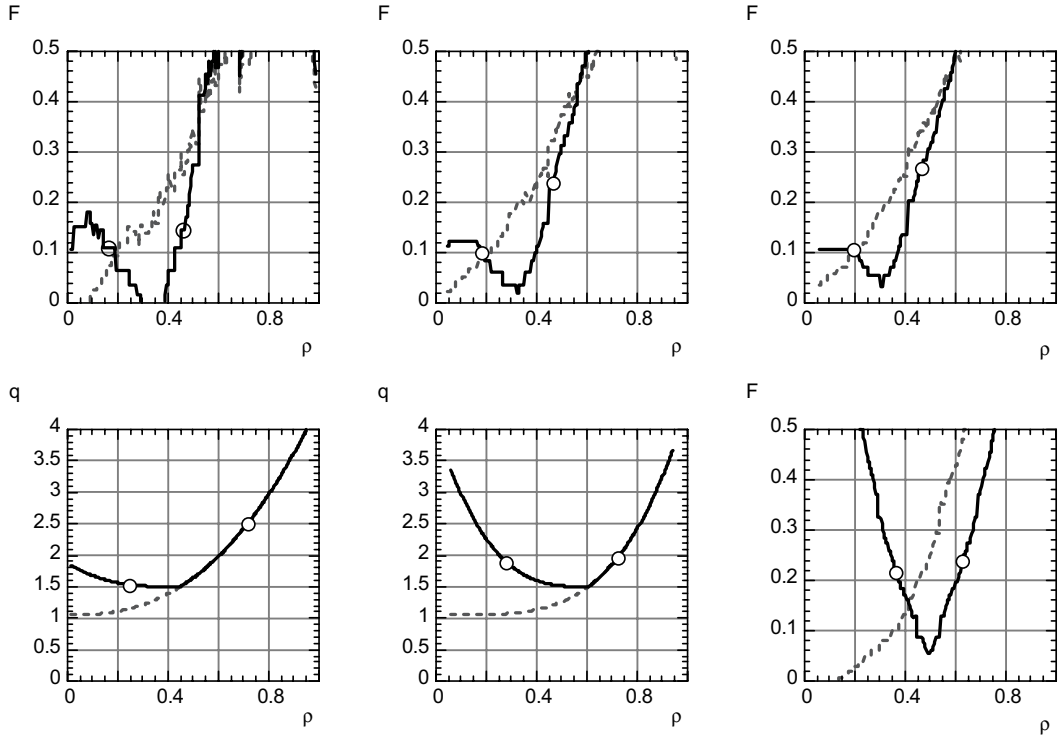

Figure 3. Top row—function representing the density of rational surfaces (circular plasmas) for parameters of ITER, JET and AUG (left to right), for q profiles shown at bottom left (dashed lines for normal, solid lines for flattened profile). Bottom right—function representing the density of rational surfaces for AUG for less flat q profiles shown in centre.

3. Improved H-modes

Improved H-modes, characterized by low magnetic shear with central q close to but somewhat larger than unity, have been achieved in AUG with off-axis current drive by neutral beams [13]. Similar conditions have also been obtained in DIII-D [14], JET [15] and JT-60 [16]. Such H-modes are considered promising candidates for obtaining improved confinement in ITER.

A possible mechanism to explain this improved confinement is the reduction of turbulent transport in regions for which the low order rational q surfaces are sparse, as proposed in [17] and studied in [18, 19]. In order to investigate this hypothesis by modelling, we have implemented this stabilization mechanism by defining a function that depends on the difference of the spatial distribution of low-order rational surfaces for a reversed or flat q profile as compared with the normal profile. 'Low-order rational' surfaces are defined as those for which the number of toroidal circuits to field line closure is not large (about below ten). The sparseness function is given by the number of rational surfaces within a characteristic radial width from the surface under consideration, weighted by the inverse of the product of the number of toroidal circuits times the distance from the surface. The function is normalized to its integral over the radius. The characteristic width used is proportional to a mixing length $\sim\sqrt{\rho_{\mathrm{i,tor}} \cdot R}$ (e.g. [17]). (Similar results are obtained if the characteristic length is taken to be $\sim\sqrt{\rho_{\mathrm{e,pol}} \cdot a}$.) As an example, we show in figure 3 the sparseness function calculated for analytic q profiles for circular plasmas with major and minor radii corresponding to the AUG, JET and ITER. The q profiles are similar to those of [19], figures 11 and 13. It is seen that the function provides a reasonable discrimination between normal and reversed or flat q profiles at a value of 0.1 to 0.15 for all three machines.

In the simulations, the local value of the sparseness function f_{rat} defined above is calculated from the profiles obtained in the simulation, with the full (non-circular) equilibrium obtained by Astra using a moment expansion. The effect of the sparseness of rational surfaces is implemented by multiplying the transport by a predetermined factor F when the function f_{rat} drops below a threshold value of 0.1 (no confinement improvement is applied for q values close to unity because sawteeth act there):

$$\chi_{\mathrm{IHM}} = F \cdot \chi_{\mathrm{norm}} \qquad \text{when} \quad f_{\mathrm{rat}} \leqslant 0.1,$$
$$\chi_{\mathrm{IHM}} = \chi_{\mathrm{norm}} \qquad \text{when} \quad f_{\mathrm{rat}} > 0.1,$$

where χ_{IHM} is the transport in improved H-mode and χ_{norm} that without reduction owing to the sparseness of rational surfaces. The strength of the stabilization to be used is deduced from AUG parameters approximating those of discharge #15524 as given in [13]. Figure 4 shows the resulting profiles for four conditions: normal q profile, flattened q profile without additional reduction, reduction factor $F = 1/5$ and reduction factor $F = 1/10$. For the same heating power profile (2.5 MW on axis, 2.5 MW at mid-radius), the H factor (H98y2) in AUG rises by 26% for $F = 1/5$ and by 31% for $F = 1/10$ with respect to its value of 1.02 for the normal q profile (of this, the flattening of the q profile before application of the reduction factor alone accounts for 11%). The corresponding H factor in the experiment is ~1.3, so F in the range of 0.1 to 0.2 appears appropriate.

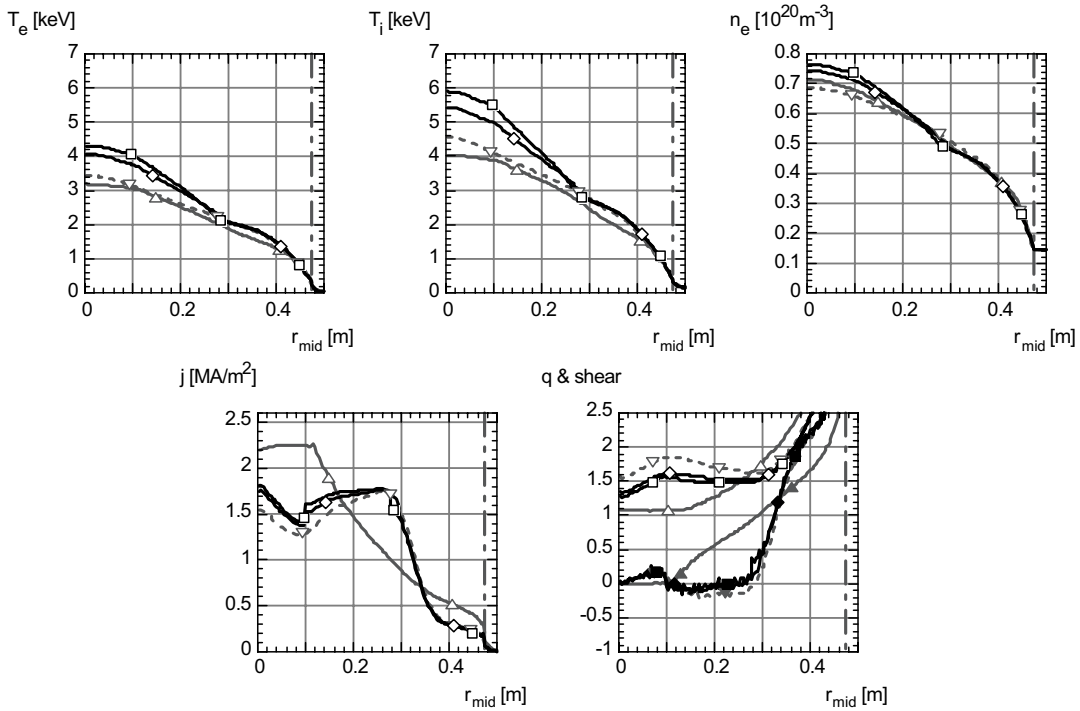

Figure 4. Simulation for Asdex-UG parameters ($B = 2.47\,\mathrm{T}$, $I = 1\,\mathrm{MA}$), showing radial profiles of: electron (top left) and ion temperature (top centre) and density (top right); current density (bottom left), q and shear (bottom right, q = hollow, shear = filled). All profiles for same heating power: solid grey: normal current profile, dotted grey: ∼0 shear, black lozenges: ∼0 shear with transport reduction of $\frac{1}{5}$, black squares: ∼0 shear with transport reduction $\frac{1}{10}$.

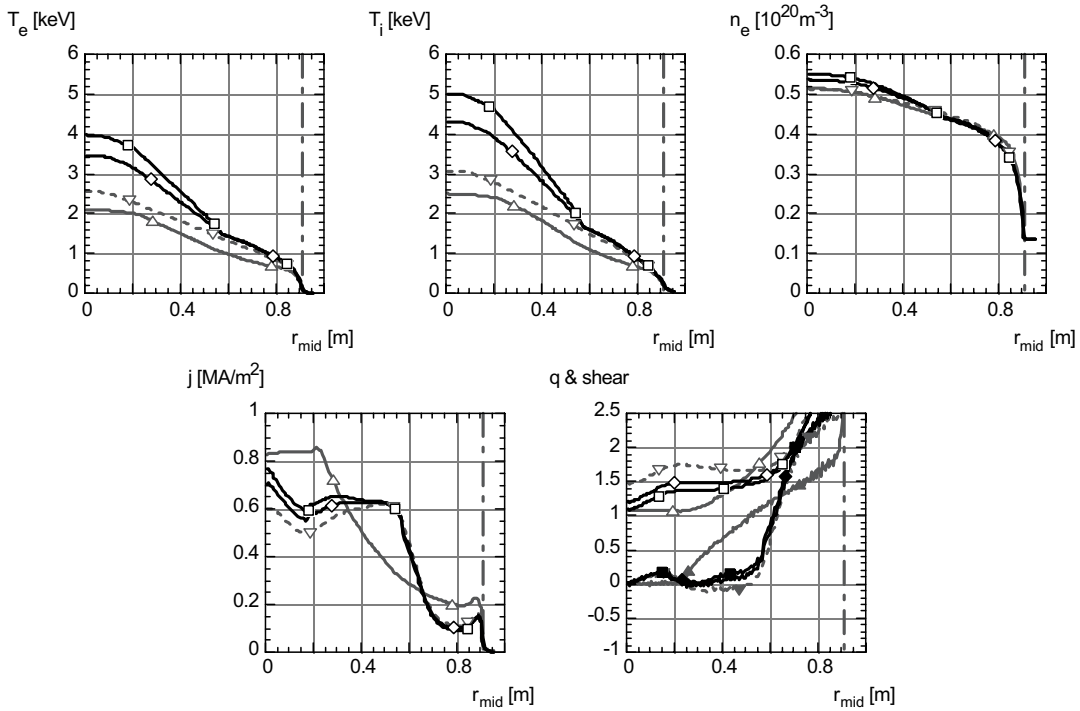

Figure 5. Simulation for JET parameters ($B = 1.7\,\mathrm{T}$, $I = 1.4\,\mathrm{MA}$, $P = 8\,\mathrm{MW}$). Arrangement of figures and legend as in figure 3.

The same technique is applied for JET parameters with the same edge q as for the AUG discharge (figure 5). The heating profile is taken to be fairly broad and centred on axis with a total beam power of 8 MW. In order to facilitate the comparison between machines, a similar flattened q profile as in AUG is imposed by adding a non-inductively driven current. In order to isolate the effect on transport of changing the current distribution, the driven current is applied without

changing the power deposition profile (which remains centred and equal to 8 MW). Since the additional current profile is not aligned with the heating profile, this supposes that a part of the current profile is established during rampup and frozen in thereafter (in addition, the current drive efficiency which would be required for the 8 MW of heating power to produce the non-inductive current would be 0.9×10^{19} A W^{-1} m^{-2}, higher than that usually obtained). For these conditions, the H factor (H98y2) in JET rises to 1.05 (64% increase) for $F = 1/5$ and to 1.13 for $F = 1/10$ with respect to its value of 0.64 for the normal q profile (the flattened q profile alone gives 0.83). The improvement in H factor for the case $F = 1/5$ is comparable to the experimental result reported in [15].

Thus, the main feature of the improved H-mode, improved confinement on a large radial extent at low shear, is reproduced by this model for both these devices. However, it should be pointed out that the $E \times B$ stabilization applied to the edge to obtain the pedestal is only applied there and not in the main part of the plasma, and that the $E \times B$ stabilization included in the MMM model was not yet activated; this remains to be done but is not expected to be very important for these conditions because the transport is already largely reduced by the effects discussed above.

In the course of this work, we have also applied the model to conditions for which a hot ion H-mode would be obtained in JET [20]. In a first preliminary investigation, the model (which contains MMM transport) included $E \times B$ stabilization over the entire profile but did not take into account the stabilization resulting from the sparseness of rational surfaces discussed above. In these conditions, a hot ion H-mode was not obtained in the simulations since the ratio of ion to electron temperatures remained well below 2 even when equipartition was turned off for demonstration purposes.

Similarly, in the improved H-mode simulation described above, an increase of the heating power to 20 MW (as in the second stage of discharge 58323 described in [15]) resulted in a ratio of central ion temperature to electron temperature of only 1.4, rather than over 2 as observed in the experiment, even though the improvement in the H factor was similar to the observations. Further simulations should thus be undertaken to determine how the model of ion transport included in the MMM model should be amended to reduce the underlying ion transport under these conditions.

4. Application to ITER parameters

For application to ITER, we have investigated conditions with current profiles similar to those of AUG and JET above. The examples discussed have 50 MW of additional heating and a total current of 12 MA, resulting in an edge q of ~4.5. This would require a part of the current profile to be established and frozen in during rampup and the remainder to be produced by current drive at rather high efficiency, $\sim 3.5 \times 10^{19}$ A W^{-1} m^{-2}.

The resulting profiles are shown in figure 6 for an average density of ~90% of the Greenwald limit n_{GW}. When the stabilization owing to the sparseness of rational surfaces is applied, both electron and ion temperatures rise and the H factor increases by 20% (from H98y2 = 1.25 to 1.47); half of this results directly from the flattened q profile, and the other half comes from the transport reduction by a factor of five in the flat q region.

Despite the improved confinement demonstrated here, the fusion power does not increase with the transport reduction when the full ICPS model as described in [4] is used because of carbon accumulation. Carbon is included as an impurity, with the neoclassical equilibrium impurity profile determined according to the formulae of [10] recapitulated below:

$$n_C(r) = n_{C\text{-sep}} \exp\left\{\int_a^r \left(\frac{v_{an} + v_{coll}}{D_{an} + D_{coll}}\right) dr\right\},$$

$D_{an} = 0.1(\chi_e + \chi_i)$, v_{an} assumed zero,

$D_{coll} = D_{\text{Pfirsch-Schlüter}} + D_{\text{banana-plateau}}$,

$$v_{coll} = -Z\left\{D_{\text{Pfirsch-Schlüter}}\left(\frac{1}{L_n} - \frac{1}{2L_T}\left(1 - \frac{1}{Z}\right)\right) + D_{\text{banana-plateau}}\left(\frac{1}{L_n} + \frac{3}{2L_T}\left(1 - \frac{1}{Z}\right)\right)\right\} + v_{\text{Ware pinch}},$$

L_n, L_T—gradient scale lengths for density and ion temperature,

where the anomalous diffusion coefficient is taken to be $0.1(\chi_e + \chi_i)$ (as noted above, this value gave good agreement of the density profiles with experiment). In integrated modelling, the central carbon density therefore increases as the anomalous diffusion coefficient is reduced. The resulting dilution even reduces the alpha heating power density somewhat (figure 6) despite the increase in central temperature. The corresponding total fusion power goes from 260 MW with the normal profile to 210 MW with improved confinement. It should be noted that only equilibrium impurity profiles are used in the simulation. A time-dependent calculation would therefore give higher fusion powers transiently, which would relax as the impurity accumulates, with a transition time which remains to be determined.

However, it should be possible to find conditions for which the impurity accumulation, and the resulting degradation of fusion gain, is less strong than that obtained above. On the one hand, instabilities such as the fishbones observed for flat q profiles may limit impurity accumulation without seriously affecting confinement [15]. On the other hand, active measures could be envisaged to reduce or eliminate impurity accumulation, such as central electron heating, a method which has already been successfully applied to prevent impurity accumulation in AUG [13].

To evaluate potential improvements if impurity accumulation can be controlled, a further set of simulations has been carried out. If the additional accumulation associated with stabilization via the sparseness function can be avoided a fusion power of 325 MW is obtained at $0.9\,n_{GW}$. If passive or active mitigation is successful in maintaining the carbon profile similar to that obtained for the normal current profile case, the peak alpha heating power density increases (figure 7). The corresponding total fusion power then rises from 260 MW to 436 MW ($Q \sim 5$ initially in this low-current case, rising to $Q \sim 8.5$ in the improved H-mode condition).

5. Conclusions

Improvements in the electron heat transport model and the description of the beam particle source have been implemented

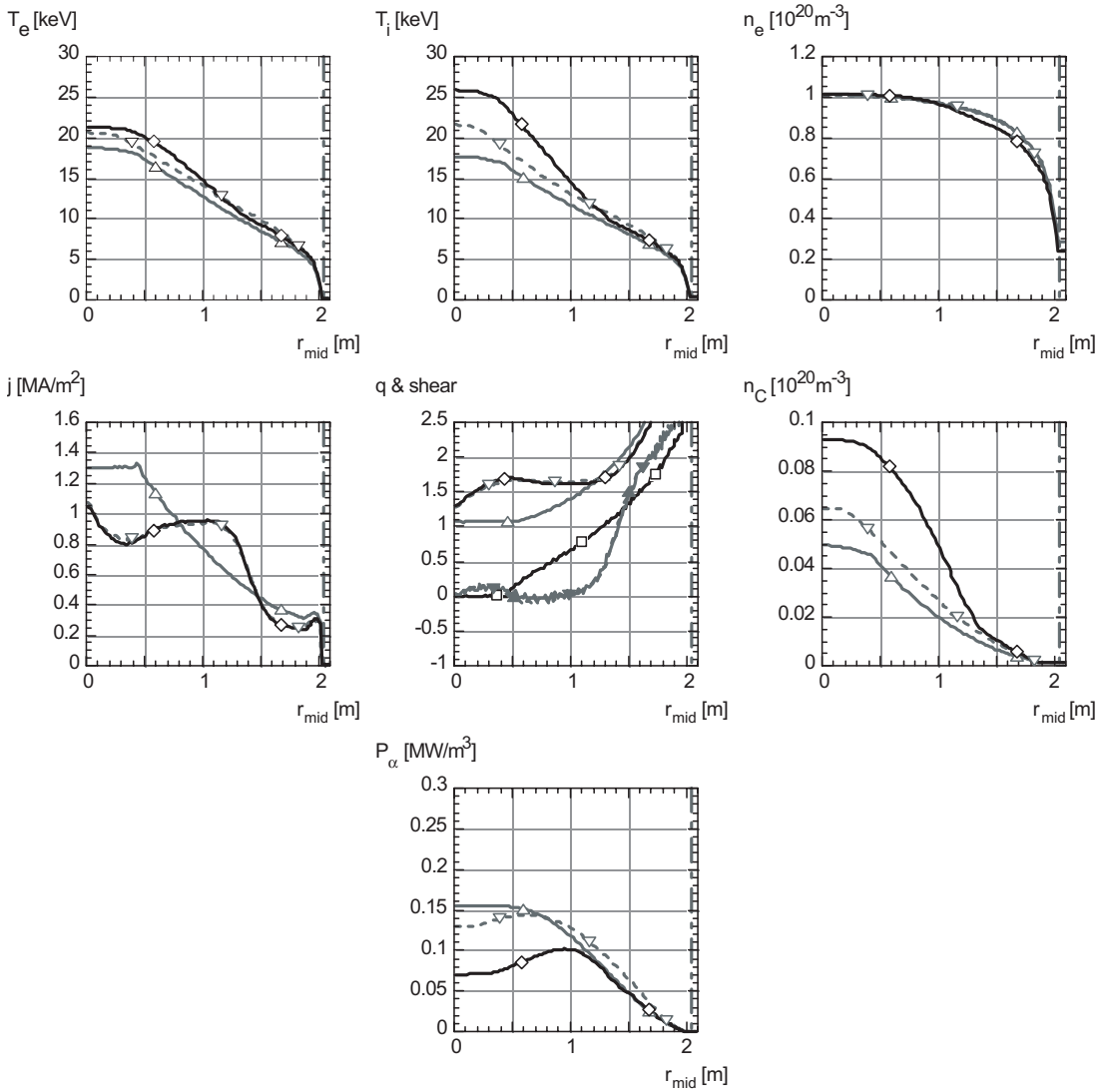

Figure 6. Simulation for ITER parameters ($B = 5.3\,\mathrm{T}$, $I = 12\,\mathrm{MA}$) showing radial profiles of: top row—electron (left) and ion temperature (centre), and density (right), middle row—current density (left), q and shear (centre) and carbon density (right). Bottom picture shows the alpha heating power density. All profiles are for the same additional heating power: solid grey: normal current profile, dotted grey: $\sim$0 shear, black lozenges: $\sim$0 shear with transport reduction of $\frac{1}{5}$.

and have led to improved agreement between the simulations and the Asdex-UG database for H-mode pedestal parameters.

Modelling of improved H-modes has commenced. The mechanism investigated is based on stabilization related to the sparseness of rational surfaces which is characteristic of flat q profiles. This mechanism is implemented in the integrated ICPS model, with parameters adjusted to simulate improved H-modes as obtained in Asdex-UG. The same model applied to JET then gives reasonable agreement for the increase of the H factor observed in improved H-modes.

However, initial application of the model to a different set of conditions, which would normally lead to ions appreciably hotter than electrons, is not yet satisfactory, and modifications of the underlying ion transport model should be investigated in future work.

The model, as used for the improved H-mode conditions of AUG and JET, has been applied to ITER, with the same flattened q profile as obtained in the Asdex-UG and JET simulations, representing ITER conditions for which the flattened q profile is established during rampup and the resistive diffusion on the resistive time scale is counteracted by current drive. In ITER, improved confinement is obtained, but the fusion power decreases in equilibrium because of neoclassical accumulation of the intrinsic carbon impurity (carbon is assumed to be present in ITER for these simulations) in the integrated model in which energy and particle confinement improve simultaneously. During the transition time towards equilibrium impurity accumulation, the fusion power would be appreciably higher than for the normal q profiles. If passive or active mitigation measures to reduce impurity accumulation are effective, a fusion power larger than 400 MW at Q values near 10 could be obtained in these conditions.

Further work will concentrate on detailed improvement and validation of the stabilization model, validation of the impurity accumulation and implementation of time-dependent

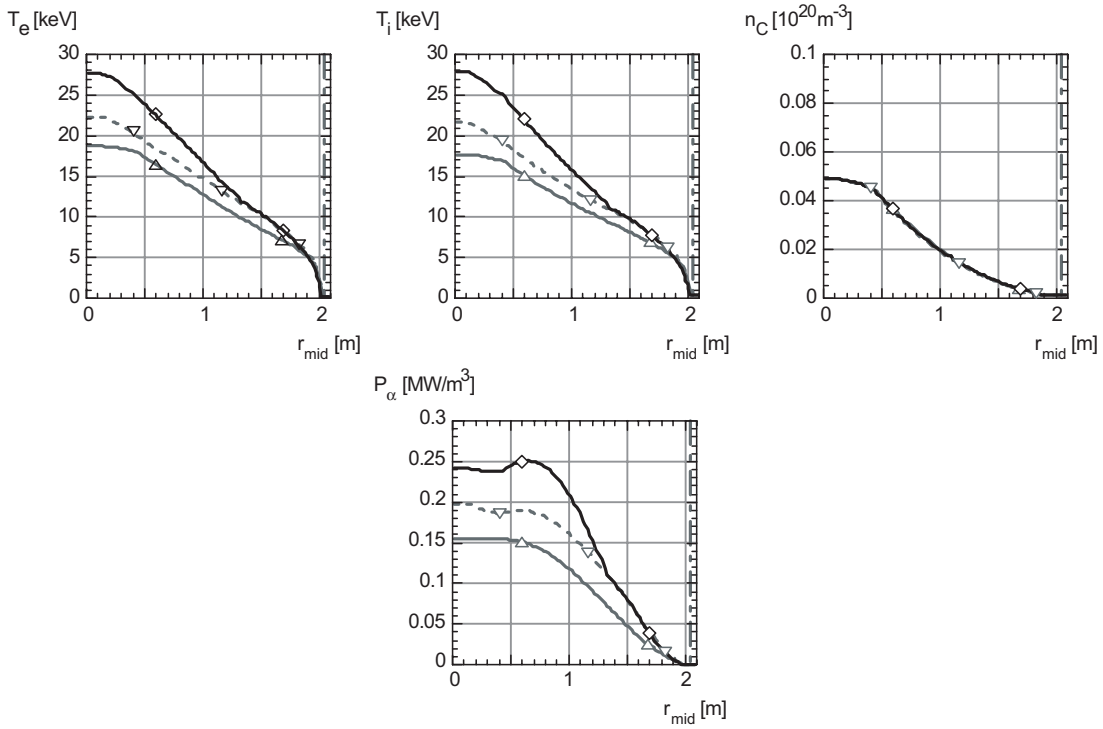

Figure 7. Simulation for ITER parameters ($B = 5.3$ T, $I = 12$ MA). For demonstration purposes (see text), the carbon density profile is constrained to remain constant as the current profile is changed and the stabilization is applied. Shown are radial profiles of: top—electron (left) and ion temperature (centre) and carbon density (right). Density, current density, q, and shear profiles are as in figure 5. Bottom picture shows the alpha heating power density. All profiles are for the same additional heating power: solid grey—normal current profile, dotted grey—∼0 shear, black lozenges—∼0 shear with transport reduction of $\frac{1}{5}$.

impurity transport and optimization of improved H-mode scenarios for ITER.

References

[1] Janeschitz G. *et al* 2002 *Plasma Phys. Control. Fusion* **44** A459–71
[2] Pacher G.W. *et al* 2003 *Nucl. Fusion* **43** 188
[3] Pacher G.W. *et al* 2003 *30th EPS Conf. on Controlled Fusion and Plasma Physics (St. Petersburg, Russia, 2003)* vol 27A (ECA) p 3.139
[4] Pacher G.W. *et al* 2004 *Plasma Phys. Control. Fusion* **46** A257–64
[5] Bateman G. *et al* 1998 *Phys. Plasmas* **5** 1793
[6] Bateman G. and Kritz A.H. http://w3.pppl.gov/NTCC/MMM95/
[7] Hirshman S.P. 1988 *Phys. Fluids* **31** 3150
[8] Pacher H.D. *et al* 2003 *J. Nucl. Mater.* C **313–316** 657
[9] Kukushkin A.S. *et al* 2005 *J. Nucl. Mater.* **337–339** 50
[10] Fussmann G. *et al* 1991 *Plasma Phys. Control. Fusion* **33** 1677
[11] Pankin A. *et al* 2005 *Plasma Phys. Control. Fusion* **47** 483
[12] Horton W. *et al* 2000 *Phys. Plasmas* **7** 1494
[13] Sips A.C.C. *et al* 2002 *Plasma Phys. Control. Fusion* **44** B69–83
[14] Wade M. R. *et al* 2002 *29th EPS Conf. on Controlled Fusion and Plasma Physics (Montreux, Switzerland, 2002)* vol 26B (ECA) O-2.8
[15] Sips A.C.C. *et al* 2003 *30th EPS Conf. on Control. Fusion and Plasma Phys. (St. Petersburg, Russia, 2003)* vol 27A (ECA) O-1.3A
[16] Isayama A. *et al* 2002 *19th IAEA Conf. on Fusion Energy (Lyon, France, 2002)*
[17] Romanelli F. and Zonca F. 1993 *Phys. Fluids* B **5** 481
[18] Garbet X. *et al* 2001 *Phys. Plasmas* **8** 2793
[19] Voitsekhovitch I. *et al* 2002 *Phys. Plasmas* **9** 4671
[20] Balet R. *et al* 1998 *25th EPS Conf. on Control. Fusion and Plasma Phys. (Prague, Czech Republic, 1998)* vol 22C (ECA) pp 325–8